

BEAM MEASUREMENTS OF THE SPS LONGITUDINAL IMPEDANCE

A. Lasheen*, E. Shaposhnikova, CERN, Geneva, Switzerland

This contribution is an extract from the following article published in Phys. Rev. Accelerators and Beams [1].

Abstract

Longitudinal instabilities are one of the main limitations in the CERN SPS to reach the beam parameters required for the High Luminosity LHC project. In preparation to the SPS upgrade, possible remedies are studied by performing macroparticle simulations using the machine impedance model obtained from electromagnetic simulations and measurements. To benchmark the impedance model, the results of simulations are compared with various beam measurements. In this study, the reactive part of the impedance was probed by measuring the quadrupole frequency shift with intensity, obtained from bunch length oscillations at mismatched injection into the SPS. This method was applied over many last years to follow up the evolution of the SPS impedance, injecting bunches with the same bunch length. A novel approach, giving significantly more information, consists in varying the injected bunch length. The comparison of these measurements with macroparticle simulations allowed to test the existing model and identify some missing SPS impedance and to obtain its possible dependence on frequency.

INTRODUCTION

One of the main challenges for future physics projects relying on particle accelerators is the need for high beam intensity, which can be limited by different collective effects. The High Luminosity LHC (HL-LHC) project at CERN needs twice higher beam intensity than achieved so far [2]. The Super Proton Synchrotron (SPS) is the last accelerator of the LHC injector chain and is the main bottleneck in terms of intensity due to beam loading and longitudinal instabilities. As the required step in performance in the SPS is high, one of the goals of the LHC Injector Upgrade (LIU) project [3] is to identify the sources of this limitation and find solutions.

The instabilities are driven by the interaction of the beam with its environment. Changes in the vacuum chamber geometry lead to electromagnetic perturbations, modeled by a beam coupling impedance \mathcal{Z} . An accurate impedance model of the ring is needed to identify the most critical contribution. A survey of all elements in the machine has been done and their impedance was found using electromagnetic simulations and bench measurements. It includes now the contribution from most of the significant sources, such as the Traveling Wave RF cavities (TWC) and their High-Order Modes (HOM), the injection/extraction kickers, the vacuum flanges (the biggest contributors correspond to the type near the focusing magnets QF), the pumping ports, and many other smaller sources [4,5]. At low energy in the

SPS, longitudinal space charge $(\text{Im}\mathcal{Z}/n)_{\text{SC}}$ is not negligible and needs to be correctly evaluated [6]. The present SPS impedance model is used in beam dynamics simulations and is presented in Fig. 1.

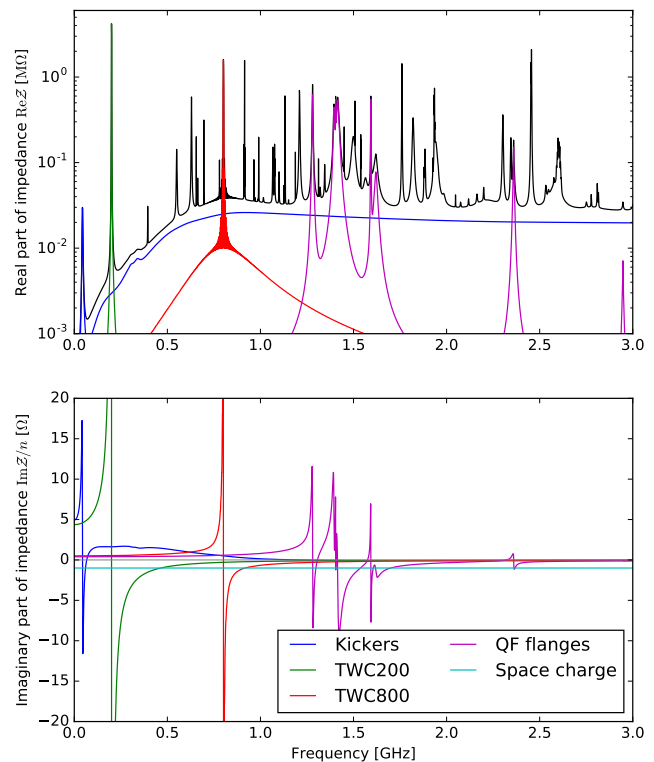


Figure 1: The present SPS longitudinal impedance model (top: resistive part, bottom: reactive part). The total impedance is represented in black (only for the real part for clarity purposes) while subsets are shown in various colors

The comparison of beam measurements performed to probe the whole impedance with macroparticle simulations can give indications about the completeness of the impedance model. The reactive part of the machine impedance can be evaluated from the measurements of the synchrotron frequency shift with intensity. Various approaches were used in different accelerators. For example, the Peak-Detected Schottky signal (e.g. in the LHC [7]), or measurements of the beam transfer function (e.g. in the PS [8]) can be used to directly observe the synchrotron frequency distribution, and the frequency shift is obtained by scanning the bunch intensity.

The method presented below relies on the measurements of bunch length oscillations at injection, initiated by a mismatched RF voltage. The frequency of these oscillations f_{s2} is approximately twice the linear synchrotron frequency and depends on the reactive part of the impedance as well as on the bunch intensity and length. Examples of recent measure-

* alexandre.lasheen@cern.ch

ments performed using bunches with different parameters are shown in Fig. 2.

The synchrotron frequency depends on the voltage seen by the beam, which is modified due to the voltage induced in the impedance sources. For bunches performing coherent oscillations, the induced voltage contribution coming from the stationary part of the bunch distribution can be separated from the one coming from the mismatched part. The frequency of coherent oscillations can be presented in the following form [9]:

$$f_{s,m}(N_b) \approx m f_{s0} + m \Delta f_{\text{inc}}(N_b) + \Delta f_{\text{coh},m}(N_b), \quad (1)$$

where N_b is the bunch intensity (number of particles in the bunch ppb), m is the mode of the oscillations ($m = 1$ is dipole or bunch position oscillations, $m = 2$ is quadrupole or bunch length oscillations), f_{s0} is the synchrotron frequency for small amplitude of oscillations, Δf_{inc} is the incoherent frequency shift due to induced voltage from the stationary bunch distribution and $\Delta f_{\text{coh},m}$ the coherent frequency shift defined by the perturbation due to the mismatched part. For dipole oscillations, the coherent and the incoherent shifts are exactly compensating each other for a parabolic bunch [10, Section 6.4] (which is a common distribution for proton bunches in the SPS), meaning that no information could be extracted so bunch length oscillations are used in this case.

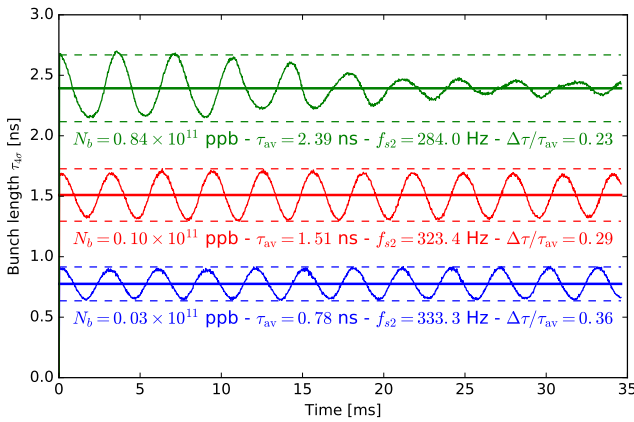


Figure 2: Examples of bunch length oscillations at SPS injection measured in the Q26 optics for different average bunch lengths τ_{av} and intensities N_b .

Since 1999, this method was used to monitor the evolution of the SPS impedance as many pieces of equipment were shielded, removed or installed [11]. The evolution of the measured quadrupole frequency shift with intensity is shown in Fig. 3 (represented by the slope b). In 1999, the main impedance contribution was from the pumping ports and the measured shift as a function of intensity was large ($b = -5.6$ Hz). The pumping ports were also the source of microwave instability in the SPS, a major limitation to reach the required beam parameters for the LHC. Therefore, their impedance was reduced by shielding in 2000. In 2001, the measured quadrupole frequency shift was lower ($b = -1.8$ Hz), proving that the impedance reduction was

successful. The shift with intensity was measured several times between 2003 and 2007 after the installation of kicker magnets for extraction to the LHC (2003 and 2006), followed by their impedance reduction (2007). However, while the large changes were easy to see, the small variations in the quadrupole frequency shift were difficult to measure. Studies showed that the measured shift b also strongly depends on the longitudinal emittance, and the lack of reproducibility in the average bunch length during measurements led to inconsistent results (e.g. the measured shift b increased in 2007, although the SPS impedance was reduced).

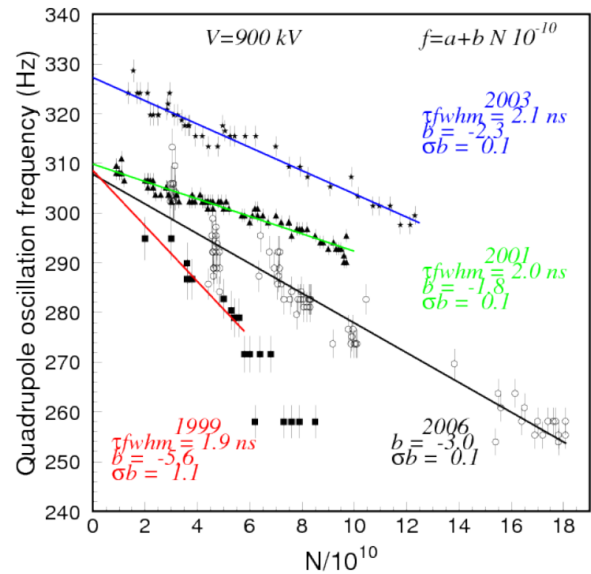


Figure 3: Measurements of the quadrupole synchrotron frequency shift at 26 GeV/c in the SPS since 1999 [11].

During the Machine Development (MD) sessions of 2016, measurements were extended to scanning both the bunch intensity and the average bunch length. The dependence on bunch length could be used to extract additional information about the frequency characteristics of the SPS impedance. By comparing measurements with macroparticle simulations using the present SPS impedance model, deviations were exploited to estimate possible missing impedance contributions.

MEASUREMENTS OF THE QUADRUPOLE FREQUENCY SHIFT

Setup

The quadrupole oscillation frequency f_{s2} was measured at injection in the SPS (kinetic energy $E_k = 25$ GeV) and its dependences were analyzed by exploring a broad range of bunch intensities and lengths. The RF parameters in the SPS injectors were adjusted to scan the injected bunch properties [12]. In the SPS, the RF voltage was set for the injected bunch to be slightly mismatched hence initiating bunch length oscillations. The dipole oscillations were re-

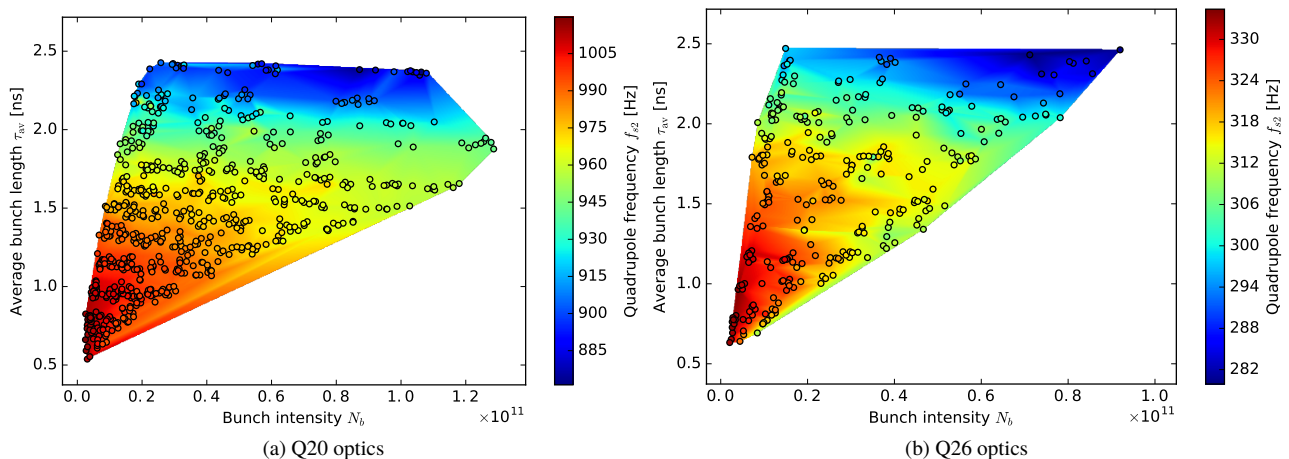


Figure 4: Measured quadrupole frequency f_{s2} as a function of bunch length and intensity in both Q20 (left) and Q26 (right) optics. Each point corresponds to a single measurement, and the colored surface corresponds to the quadrupole frequency.

duced thanks to the RF phase loop and this effect is considered negligible below. The longitudinal bunch profiles were acquired every turn using a Wall Current Monitor for an amount of turns covering approximately ten quadrupole oscillations periods.

The measured bunch length is increased, mainly due to the perturbation from the cables between the Wall Current Monitor and the oscilloscope used for the measurements. The perturbation from the Wall Current Monitor on bunch length is negligible, and the perturbation from the cables transfer function is small: the measured bunch profile is lengthened by 5-10%. The lengthening comes from short coaxial cables in the measurement line, the main part of the cables consist in a long fiber optic link, which has a negligible impact on the measured bunch profile. The Wall Current Monitor and cables transfer functions were measured, and the bunch profile was systematically corrected [13, 14]. The profiles were fitted with the binomial function

$$\lambda(\tau) = \frac{2\Gamma(3/2 + \mu)}{\tau_L \sqrt{\pi} \Gamma(1 + \mu)} \left[1 - 4 \left(\frac{\tau}{\tau_L} \right)^2 \right]^\mu, \quad (2)$$

$$\lambda(|\tau| > \tau_L/2) = 0,$$

where τ_L is the full bunch length, and where $\mu = 3/2$. The bunch length for the rest of the paper is defined as $\tau_{4\sigma} = 4\sigma_{\text{rms}}$, where σ_{rms} is the rms bunch length of the fitting profile. We note τ_{av} and $\Delta\tau$ corresponding to the average bunch length and the peak-to-peak amplitude of the bunch length oscillations. The frequency of the bunch length oscillations f_{s2} was obtained from the maximum component of the Fast Fourier Transform. The bunch intensity N_b was measured using a DC Beam Current Transformer and an averaged value was taken. Finally, each acquired SPS cycle associates the quadrupole frequency f_{s2} with an average bunch length τ_{av} , a peak-to-peak amplitude of oscillations $\Delta\tau$ and a bunch intensity N_b . Examples of these acquisitions were shown in Fig. 2.

Two different optics are available in the SPS, named after the transverse tune: Q20 and Q26. The main difference is the different γ_t and therefore a different synchrotron frequency for the same bucket area \mathcal{A}_b . Another difference is the longitudinal space charge effect which is larger in the Q26 optics with respect to the Q20 optics. This is due to the different dispersion function which gives a smaller horizontal bunch size in the Q26 optics for the same transverse emittance [6]. Measurements were performed in both optics, for the same bucket area (by adjusting the RF voltage V_{RF}) The raw data of the quadrupole frequency as a function of intensity and the average bunch length is shown in Fig. 4. The corresponding beam and machine parameters are shown in Table 1.

Table 1: The SPS beam and machine parameters for the two different SPS optics.

Optics	γ_t	V_{RF} [MV]	f_{s0} [Hz]	\mathcal{A}_b [eVs]	$\left(\frac{\text{Im}Z}{n}\right)_{\text{SC}}$ [Ω]
Q20	17.95	2.8	517.7	0.473	-1.0
Q26	22.77	0.9	172.4	0.456	-1.27

Data analysis and results

The dependence of the quadrupole frequency f_{s2} on intensity was studied by selecting the data with the same average bunch length τ_{av} (within ± 50 ps). For each set, the dependence on intensity is obtained from the fit by a linear function $f_{s2} = a + b N_b$. The origin of the fit a corresponds to the quadrupole frequency without intensity effects, while the slope b contains the information about the reactive impedance. Examples of measured quadrupole frequency f_{s2} as a function of intensity for different sets of average bunch length τ_{av} together with fits are shown in Fig. 5.

The dependence of the quadrupole frequency on bunch length can be studied from the fitted parameters a and b

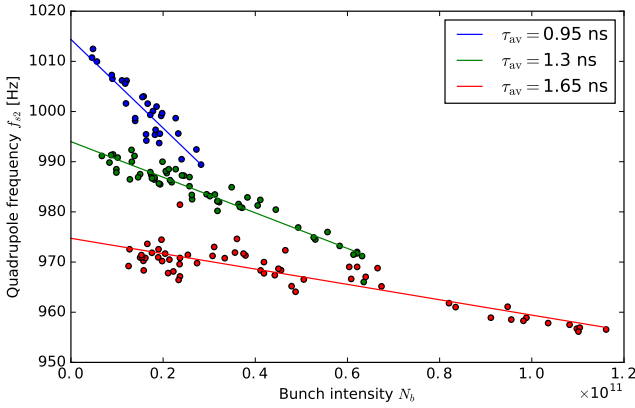


Figure 5: Examples of measured quadrupole frequency f_{s2} as a function of intensity for selected average bunch lengths τ_{av} (within ± 50 ps) in the Q20 optics. The lines correspond to a linear fit.

obtained for each set of τ_{av} . The measured quadrupole oscillations are mainly performed by the mismatched particles from the outer part of the distribution. The first consequence is that the quadrupole frequency without intensity effects a (τ_{av}) should follow [1]:

$$a(\tau_{av}) \approx 2f_{s0} \left[1 - \frac{(\omega_{RF}\tau_{av})^2}{64} \right], \quad (3)$$

where $f_{RF} = \omega_{RF}/(2\pi)$ is the RF frequency and where the right-hand side of the equation is noted $2f_s^{(0)}$, which is the quadrupole frequency including the effect of the non-linearity of the RF voltage. The comparison of measurements with the expected analytical formula is shown in Figs. 6a and 6b for both optics. They are in good agreement, confirming that the measured quadrupole frequency is dominated by contributions from particles with large synchrotron oscillation amplitudes. The small discrepancy between measurements and the expected scaling comes from the fact that Eq. (3) is valid for particles with maximum oscillation amplitude, while in measurements the frequency is determined by the sum of all the particles defining the mismatch.

It is possible to extrapolate the value of $2f_{s0}$ from the measured a ($\tau_{av} \rightarrow 0$) which gives the actual amplitude of the RF voltage during measurements (this parameter has an uncertainty of $\approx 5\%$). For both Q20 and Q26 optics the measured values ($2f_{s0} \approx 1035$ Hz in the Q20 optics and $2f_{s0} \approx 342$ Hz in the Q26 optics) are in good agreement with the values expected in theory in Table 1. The measured slope b is shown in Figs. 6c and 6d and it scales approximately as $\propto 1/\tau_{av}^3$, in accordance to the expected scaling of the synchrotron frequency shift for large particle oscillation amplitudes [1].

In previous studies of the synchrotron frequency shift as a probe of the reactive impedance, only the slope b was taken to compare measurements and simulations. However, the strong dependence on bunch length of the slope b implies that small deviations in the measured bunch length could lead to important differences between measurements and

simulations (e.g. due to perturbations in the measured profile from the measurement line, see *Setup* paragraph). Therefore, it was found preferable to use as a figure of merit the equivalent impedance which dependence on bunch length is less strong, even if the measured bunch profile was corrected regarding perturbations in the measurement line. The analyzed parameters $a = 2f_s^{(0)}$ and $b = -2\Delta f_{inc}/N_b$ are recombined to obtain the equivalent reactive impedance as [1]:

$$(\text{Im}\mathcal{Z}/n)_{eq} = \frac{\omega_{rev}^2 V_{RF} h}{6q} \frac{b}{a} \tau_{av}^3, \quad (4)$$

where $f_{rev} = \omega_{rev}/(2\pi)$ is the revolution frequency, q the charge of the particles, h the RF harmonic number. The results are shown in Figs. 6e and 6f. Note that the equivalent impedances $(\text{Im}\mathcal{Z}/n)_{eq}$ are very similar for the Q20 and Q26 optics since the dependence on the machine parameters V_{RF} and η was removed.

For the measured equivalent impedance $(\text{Im}\mathcal{Z}/n)_{eq}$ we can distinguish three different bunch length intervals. For $\tau_{av} < 1.7$ ns, the results are similar in pattern and value between the Q20 and Q26 optics and correspond to the ideal bunch length range for these measurements. At $\tau_{av} \approx 1.7$ ns, the measured equivalent impedance $(\text{Im}\mathcal{Z}/n)_{eq}$ in the Q20 and Q26 optics starts to be different. For the Q20 optics, the measured values keeps decreasing increase whilst the equivalent impedance grows in the case of the Q26 optics. For $\tau_{av} > 2$ ns the measured equivalent impedance $(\text{Im}\mathcal{Z}/n)_{eq}$ in Q20 is completely unusable. This is explained by the motion of a mismatched bunch in phase space which is heavily affected by the non-linearities of the RF bucket for large bunch lengths. As shown in Fig. 2, the consequence is that the bunch profile changes with time and bunch length oscillations are quickly damped due to filamentation. In addition, the bunch is shortened in the SPS injector (PS) by a fast RF voltage increase (bunch rotation in phase space). For large bunch lengths, the distribution in phase space is distorted during the bunch rotation in the longitudinal phase space and has an "S-shape" [15], making the filamentation effects even more difficult to reproduce. Moreover, the spectrum of a filamenting bunch has components at high frequency, which could affect the synchrotron frequency shift. In those conditions the results are varying from one acquisition to another. Nevertheless, the main observation is that for large bunch lengths the equivalent impedance $(\text{Im}\mathcal{Z}/n)_{eq}$ for $\tau_{av} > 2$ ns is increasing, implying that long bunches are mainly sampling inductive impedance.

PARTICLE SIMULATIONS

BLoND simulations

The dependence of the quadrupole frequency shift on the SPS impedance can be studied more precisely by macroparticle simulations that include the RF non-linearities and induced voltage. The simulation code BLoND was written at CERN to simulate longitudinal beam dynamics in synchrotrons and was successfully benchmarked with measurements in various accelerators and physics cases. including

BEAM MEASUREMENTS OF THE SPS LONGITUDINAL IMPEDANCE

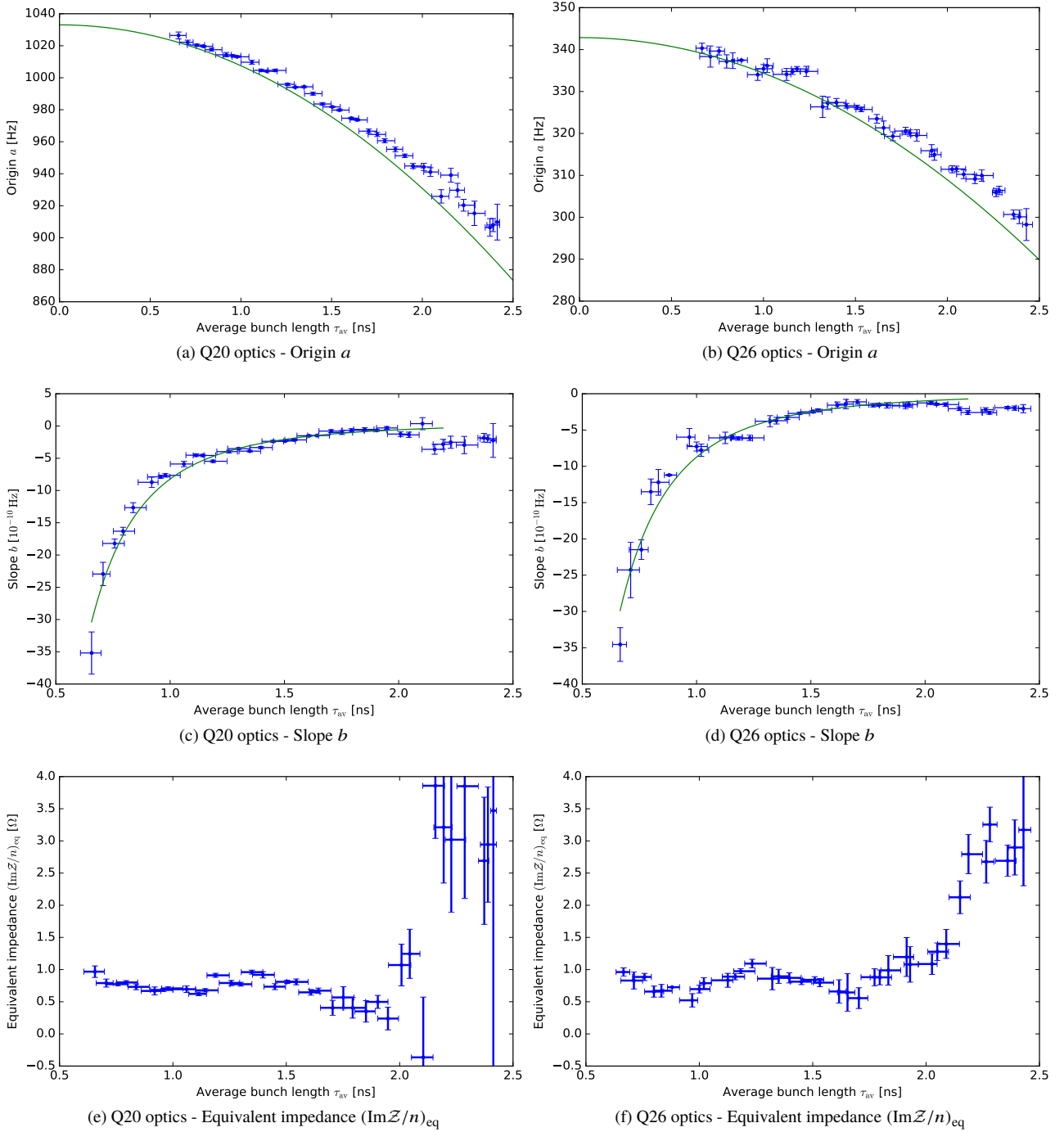


Figure 6: The fitted origin a (top), slope b (middle) and their expected scaling from theory (green, respectively from Eq. (3) and $\propto -1/\tau_{av}^3$). The Eq. (4) is used to get the corresponding equivalent impedance $(\text{Im}\mathcal{Z}/n)_{eq}$ (bottom) of the quadrupole frequency shift with intensity, as a function of the average bunch length τ_{av} , in the Q20 (left) and Q26 (right) optics.

the synchrotron frequency shift with intensity [16]. All simulations were done using the SPS impedance model presented in Fig. 1 (both resistive and reactive parts).

The SPS machine parameters were set in simulations to be the same as in measurements (for both optics in Table 1). To cover the same range of longitudinal emittances and bunch intensities obtained in measurements, each acquisition was

reproduced in simulations by taking the injected bunch profile and reconstructing the bunch distribution in phase space using the Abel transform [17]. To get in simulations a mismatch close to the one in measurements, the bunch distribution in phase space was generated and the energy spread was iteratively adjusted so that the peak-to-peak bunch length oscillations $\Delta\tau$ are similar to the corresponding acquisition.

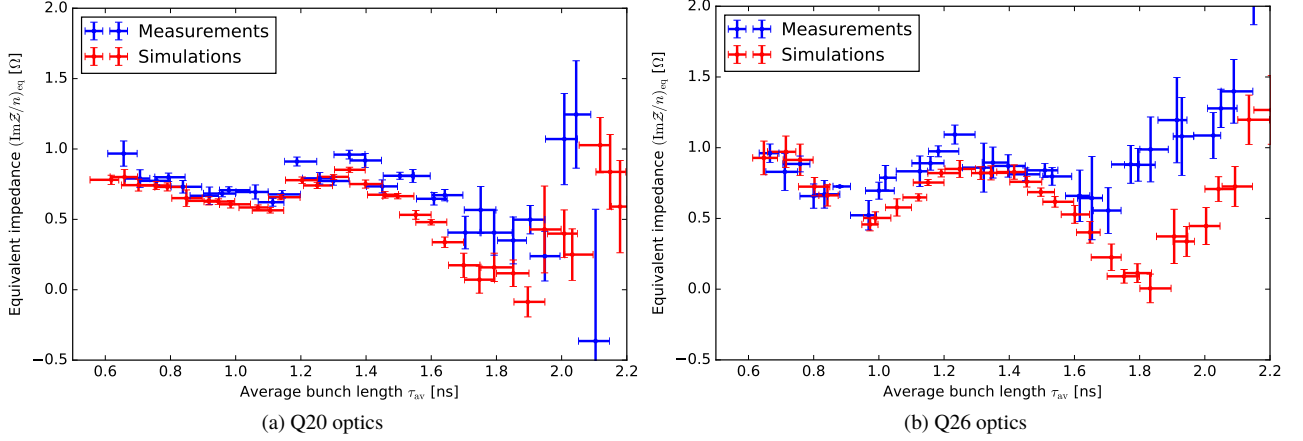


Figure 7: Equivalent impedance $(\text{Im}\mathcal{Z}/n)_{\text{eq}}$ as a function of bunch length obtained from measurements (blue) and simulations (red) using the full SPS impedance model in the Q20 (left) and Q26 (right) optics.

For small bunch lengths, this approach is good enough to get input distributions close to the ones extracted from the PS without having to simulate the bunch rotation in the PS. Simulation results analyzed applying exactly the same method as used for measurements are presented in Fig. 7.

Overall, simulations using the present SPS impedance model are in good agreement with measurements and the non-trivial dependence of the equivalent impedance $(\text{Im}\mathcal{Z}/n)_{\text{eq}}$ on bunch length is well reproduced in both optics. Nevertheless, some systematic deviations can be noticed. First, the equivalent impedance $(\text{Im}\mathcal{Z}/n)_{\text{eq}}$ is in general lower in simulations than in measurements, suggesting that some impedance is still missing in the SPS impedance model. Next, the discrepancy is higher for $\tau_{\text{av}} \approx 1.6$ ns, indicating that the missing impedance has a particular frequency dependence. The results for $\tau_{\text{av}} > 1.7$ ns are less accurate due to the limitations described above and may not be suitable to draw reliable assumptions on possible missing impedance.

Evaluation of the missing impedance

To define possible missing impedance sources, the simulations were reiterated by adding a variable amount of constant inductive impedance $\text{Im}\mathcal{Z}/n$. Results are shown in Fig. 8. The present SPS impedance including space charge is represented in blue and the deviations between measurements and simulations could be explained by an additional inductive impedance in the order of $\text{Im}\mathcal{Z}/n \approx (0 - 1.5)$ Ω depending on the bunch length. This is comparable to the longitudinal space charge impedance of $(\text{Im}\mathcal{Z}/n)_{\text{SC}} \approx -1$ Ω . Omitting the longitudinal space charge impedance in simulations would correspond to the red line. In this case, the interpretation would have been opposite, since we would have concluded that the inductive impedance in the present model is in excess. Therefore, the longitudinal space charge effects are indeed not negligible and should be included in simulations at flat bottom in the SPS. An accurate evaluation

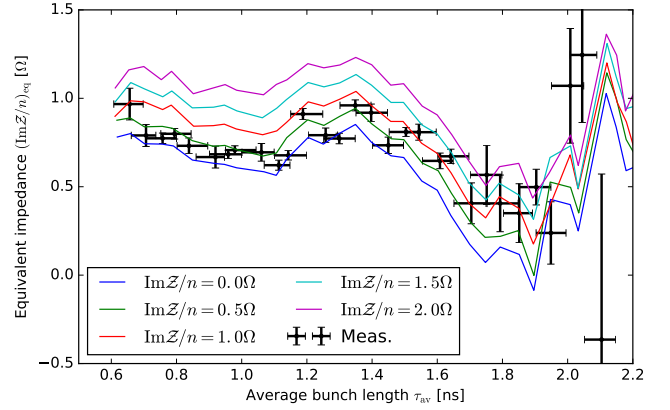


Figure 8: Measured equivalent impedance $(\text{Im}\mathcal{Z}/n)_{\text{eq}}$ (black) in the Q20 optics compared with simulations (colored lines) adding a variable amount of inductive impedance in the range $\text{Im}\mathcal{Z}/n = (0 - 2)$ Ω to the full SPS impedance model.

of the longitudinal space charge impedance was done [6], leading to the values shown in Table 1 for both optics.

By using the previous scan in simulations adding a variable amount of constant inductive impedance $\text{Im}\mathcal{Z}/n$, it is possible to determine for each bunch length the necessary impedance value to reach a perfect agreement between simulations and measurements. Results are shown in Fig. 9 for both optics.

For $\tau_{\text{av}} < 1.4$ ns, the missing impedance is constant in first coarse approximation and it is necessary to add $\Delta(\text{Im}\mathcal{Z}/n) \approx 0.3$ Ω in the Q20 optics and $\Delta(\text{Im}\mathcal{Z}/n) \approx 0.5$ Ω in the Q26 optics to remove the deviations. For this large range of bunch lengths, a broadband impedance source could be the missing contribution, as determined in the previous section. Whilst non negligible, this missing contribution is still small in comparison with the full impedance budget and could be explained by an underestimation of a source in the model or some contributions that were not included.

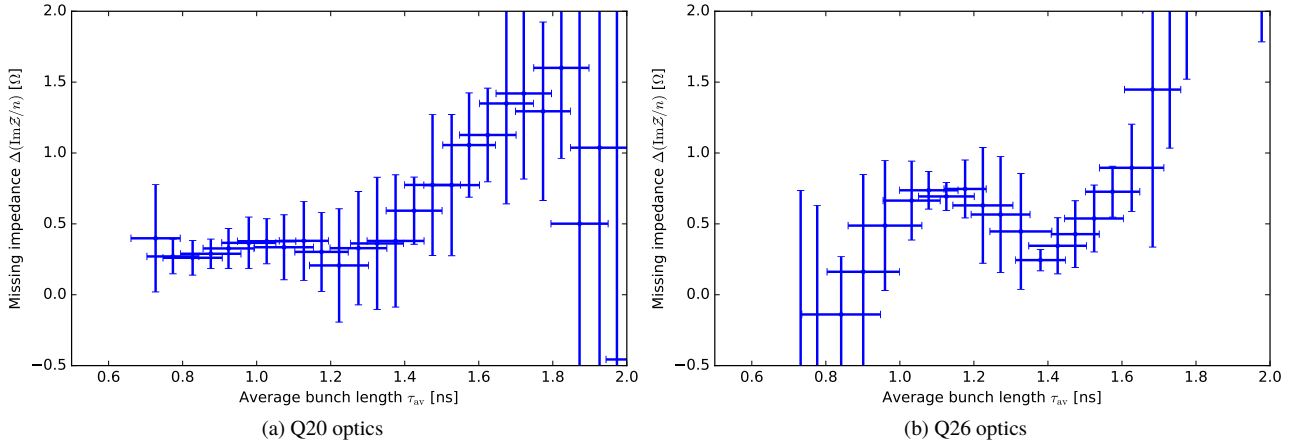


Figure 9: Missing inductive impedance $\Delta(\text{Im}\mathcal{Z}/n)$ as a function of bunch length needed to get a perfect agreement between measurements and simulations shown in Fig. 7 for both Q20 (left) and Q26 (right) optics.

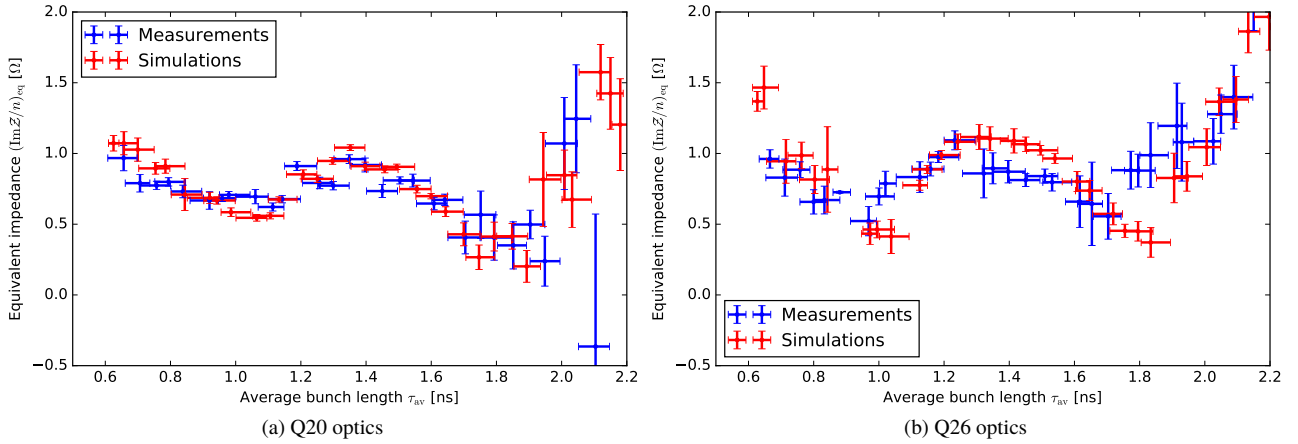


Figure 10: Equivalent impedance $(\text{Im}\mathcal{Z}/n)_{\text{eq}}$ in measurements and simulations after adding an extra resonator with $f_r = 350$ MHz, $R/Q = 3$ k Ω and $Q = 1$ to the SPS impedance model to compensate for deviations from measurements in both Q20 (left) and Q26 (right) optics.

For τ_{av} in the range (1.4 – 1.7) ns, the missing impedance is increasing linearly, suggesting that an impedance source as a resonator could also be missing. Simulations were done with an additional resonator and its resonant frequency f_r and impedance R/Q were scanned to further reduce the discrepancy (with $Q = 1$). The best agreement was found for a resonator with $f_r \approx (350 \pm 50)$ MHz and $R/Q \approx (3 \pm 1)$ k Ω , leading to an almost perfect agreement in the Q20 optics as shown in Fig. 10a. While in the Q26 optics the agreement is also improved, some small deviations are still present at $\tau_{\text{av}} \approx 1.0$ ns and $\tau_{\text{av}} \approx 1.5$ ns (see Fig. 10b). Adding a single resonator is most probably not enough to correct all the deviations between measurements and simulations. A perfect description of the missing impedance is a multi-parametric task which requires a very large amount of measured data with small error-bars. Moreover, the realistic frequency dependence of a device contributing to the machine impedance could be more complex than that of a single resonator. Nevertheless, clear indications for the

missing effective impedance as a function of bunch length can be exploited to get hint and direction for further searches. The missing contribution, depending on its frequency, could also be critical to have a reliable SPS impedance model for the bunch stability studies required for the SPS upgrade.

CONCLUSIONS

The measured quadrupole frequency shift with intensity has been used to probe the reactive part of the SPS machine impedance. Being very sensitive to the average bunch length because of the non-linearities of the RF bucket and the induced voltage, this method can nevertheless be used to have an estimate of the missing impedance and its frequency dependence. Measurements were done in the SPS in two different optics and allowed, from good agreement with particle simulations, to show that the present SPS impedance model is satisfactory to reproduce the measured synchrotron frequency shift. The agreement can be further increased by adding a resonant impedance at $f_r \approx 350$ MHz with

$R/Q \approx 3 \text{ k}\Omega$ and $Q = 1$, the real source to be investigated. As the studies for the HL-LHC project rely on the accurate reproduction of beam instabilities, any missing impedance could be crucial and this method is an effective way to test the existing impedance model. Beyond the evaluation of the longitudinal impedance model, the study of the synchrotron frequency shift is also important as it is a key component to determine the instability mechanisms related to the loss of Landau damping.

ACKNOWLEDGMENTS

We would like to thank the impedance working group at CERN for the development of the SPS impedance model and in particular T. Kaltenbacher, C. Zannini and B. Salvant. We would also like to thank T. Bohl for helping during the measurements in the SPS and S. Hancock for the help in the preparation of the necessary cycles in the PSB and PS. We are grateful to the MD coordinators for providing with beam time and the operation team for setting up the cycles. Finally we would like to thank BLonD developers for their contributions to the simulation code.

REFERENCES

- [1] A. Lasheen and E. Shaposhnikova, "Evaluation of the cern super proton synchrotron longitudinal impedance from measurements of the quadrupole frequency shift," *Phys. Rev. Accel. Beams*, vol. 20, p. 064401, Jun 2017.
- [2] G. Apollinari, I. Béjar Alonso, O. Brüning, M. Lamont, and L. Rossi, "High-Luminosity Large Hadron Collider (HL-LHC): Preliminary Design Report," Tech. Rep. CERN-2015-005, CERN, Geneva, Switzerland, Dec 2015.
- [3] H. Damerau, A. Funken, R. Garoby, S. Gilardoni, B. Goddard, K. Hanke, A. Lombardi, D. Manglunki, M. Meddahi, B. Mikulec, G. Rumolo, E. Shaposhnikova, M. Vretenar, and J. Coupard, "LHC Injectors Upgrade, Technical Design Report, Vol. I: Protons," Tech. Rep. CERN-ACC-2014-0337, CERN, Geneva, Switzerland, Dec 2014.
- [4] J. E. Campelo, T. Argyropoulos, T. Bohl, F. Caspers, J. Esteban Müller, J. Ghini, A. Lasheen, D. Quartullo, B. Salvant, E. Shaposhnikova, and C. Zannini, "An Extended SPS Longitudinal Impedance Model," in *Proceedings of IPAC2015*, no. MOPJE035, (Richmond, VA, USA), pp. 360–362, May 2015.
- [5] J. E. Campelo, "Longitudinal Impedance Characterization of the CERN SPS Vacuum Flanges," in *Proceedings of IPAC2015*, no. MOPJE036, (Richmond, VA, USA), pp. 363–365, May 2015.
- [6] A. Lasheen, "Longitudinal Space Charge in the SPS," Tech. Rep. CERN-ACC-NOTE-2016-0074, Dec 2016.
- [7] E. Shaposhnikova, T. Bohl, and T. Linnecar, "Longitudinal Peak Detected Schottky Spectrum," in *Proceedings of HB2010*, no. TUO1C04, (Morschach, Switzerland), pp. 363–367, September 2010.
- [8] M. Migliorati, S. Persichelli, H. Damerau, S. Gilardoni, S. Hancock, and L. Palumbo, "Beam-wall interaction in the cern proton synchrotron for the lhc upgrade," *Phys. Rev. ST Accel. Beams*, vol. 16, p. 031001, Mar 2013.
- [9] J. L. Laclare, "Bunched beam coherent instabilities," in *Proceedings of CAS 1985 Vol. I*, (Geneva, Switzerland), pp. 264–326, 1987.
- [10] A. W. Chao, *Physics of collective beam instabilities in high energy accelerators*. New York, NY: Wiley, 1993.
- [11] E. Shaposhnikova, T. Bohl, H. Damerau, K. Hanke, T. Linnecar, B. Mikulec, J. Tan, and J. Tückmantel, "Reference Measurements of the Longitudinal Impedance in the CERN SPS," in *Proceedings of PAC09*, no. FR5RFP056, (Vancouver, Canada), pp. 4667–4669, May 2009.
- [12] S. Hancock, "Improved Longitudinal Blow-up and Shaving in the Booster," Tech. Rep. CERN-ATS-Note-2013-040 MD, CERN, Jul 2013.
- [13] T. Bohl, "APWL-10 transfer function," Tech. Rep. Note-2006-37, CERN, 2006.
- [14] T. Bohl, "Pulse response of SPS APWL signal chain via FO Link No. 1," Tech. Rep. Note-2011-09, CERN, 2011.
- [15] H. Timko, T. Argyropoulos, T. Bohl, H. Damerau, J. F. Esteban Müller, S. Hancock, and E. Shaposhnikova, "Longitudinal transfer of rotated bunches in the cern injectors," *Phys. Rev. ST Accel. Beams*, vol. 16, p. 051004, May 2013.
- [16] H. Timko, J. E. Müller, A. Lasheen, and D. Quartullo, "Benchmarking the Beam Longitudinal Dynamics Code BLonD," in *Proc. of International Particle Accelerator Conference (IPAC'16), Busan, Korea, May 8-13, 2016*, no. 7 in International Particle Accelerator Conference, (Geneva, Switzerland), pp. 3094–3097, JACoW, June 2016. doi:10.18429/JACoW-IPAC2016-WEPOY045.
- [17] P. W. Krempf, "The Abel-type Integral Transformation with the Kernel $(t^2-x^2)^{-1/2}$ and its Application to Density Distributions of Particle Beams," Tech. Rep. CERN Note MPS/Int. BR/74-1, CERN, 1974.